Transportation Engineering 6 (2021) 100096

Contents lists available at ScienceDirect

Transportation Engineering

journal homepage: www.sciencedirect.com/journal/transportation-engineering

Geotechnical and piezoresistivity properties of sustainable cementitious stabilized sand reinforced with recycled fibres

Mohammadmahdi Abedi [a], António Gomes Correia [a,*], Raul Fangueiro [b,c]

[a] Department of Civil Engineering, University of Minho, ISISE, Campus de Azurém, 4800-058 Guimarães, Portugal
[b] Department of Mechanical Engineering, University of Minho, Campus de Azurém, 4800-058 Guimarães, Portugal
[c] Centre for Textile Science and Technology, School of Engineering, University of Minho, Guimarães, Portugal

ARTICLE INFO

Keywords:
Geotechnical properties
Self-sensing geocomposite
Smart geomaterial
Fibre reinforcement
Durability

ABSTRACT

In this study, the geotechnical and piezoresistivity properties of a sustainable self-sensing cementitious stabilised sand reinforced with recycled fibres (self-sensing cementitious geocomposite, SCG) were extensively investigated. In this route, different concentrations of recycled glass, polypropylene, and ultra-high-molecular-weight polyethylene (GF, PP, and UHMWPE) fibres were incorporated into the conductive stabilised sand with 10% cement composed of 0.17% hybrid (1:1) carbon nanotubes (CNTs) and graphene nanoplatelets (GNPs). The specimens were fabricated using the standard Proctor compaction method at optimum water content, and their mechanical, hydraulic, microstructural, durability, and piezoresistivity properties were investigated after 28 days of hydration using different laboratory test methods. The test results indicate that the maximum dry densities of all SCGs were obtained with a degree of saturation of approximately 85%. For these moisture conditions, there are well-defined relationships between the maximum dry density and strength, permeability, and ultrasonic pulse velocity for SCGs. The GF and UHMWPE fibres exhibited the best performances in terms of strength, durability in climatic cycles, as well as a reduction in permeability. A unique relationship between the ratio of tangent modulus and strength with the strain was defined for all the SCGs that can be of practical use in geocomposite. Furthermore, the piezoresistivity and sensitivity of the SCGs were also increased by reinforcing the geocomposites with fibres, due to increasing their ductility. In summary, we believe that this novel approach contributes to a new era of smart geocomposite materials in sustainable intelligent transport infrastructures.

1. Introduction

Cemented stabilised sand has been widely used in different infrastructure constructions such as roads, aircraft runways, railways, and tunnels [1–4]. However, the low ductility and weakness of cemented sand against cracking is still an important issue for sustainable application of such geocomposites [5–7]. At the microstructure level, cemented sand exhibits some inherent drawbacks and numerous nanoscale cracks. Cracks are formed during the construction process or in the service life [8]. Nanocracks join and propagate, forming microcracks over time with the ageing of materials, aggressive environmental conditions, prolonged usage, and overloading, which can contribute to the formation of macrocracks and failure of the structure [9,10]. However, early detection of such damages and proper maintenance can greatly enhance the infrastructure service life, and prevent sudden collapse [9]. Stress, strain, deformation, and damage state monitoring in civil engineering structures is commonly known as structural health monitoring (SHM) [11,12]. Despite recent progress, most SHM methods include several sensors distributed in a large area of infrastructure and may not be, in some cases, the best solution for infrastructure monitoring [9]. Amongst all SHM methods, self-sensing composites provide a more integrated, real-time, and practical solution for infrastructure damage detection, considering geomaterial properties and nature [9,10]. Self-sensing composites with intrinsic sensing capabilities are based on the piezoresistivity arising from the dispersion of conductive phases within a non-conductive phase [13,14]. During loading, the random conductive paths formed by conductive fillers are disturbed by strain and stress, leading to a change in the electrical resistivity of the composite [15–17]. Although different fibrous and nanomaterials have been used as the conductive phase, recent studies indicate that hybrid carbon nanotubes (CNTs) and graphene nanoplatelets (GNPs) can significantly increase percolation and quantum tunnelling effects, reducing the

* Corresponding author.
E-mail address: agc@civil.uminho.pt (A. Gomes Correia).

https://doi.org/10.1016/j.treng.2021.100096
Received 28 August 2021; Received in revised form 2 November 2021; Accepted 11 November 2021
Available online 18 November 2021

Table 1
Characteristics of graphene nanoplatelets (GNPs) and carbon nanotubes (CNTs) [9,10].

GNP Surface area (m^2 g^{-1})	Density (g/cm^3)	Carbon content (%)	Tensile modulus (GPa)	pH value (30 °C)	Tensile strength (GPa)	Layers	Dimension		Form	Part number
120–150	0.6	> 99.5	1000	7–7.65	5	10 < *n* < 60	Thickness 4–20 nm	Diameter 5–10 μm	Grey Powder	TGN201

MWCNT Surface area (m^2 g^{-1})	Density (g/cm^3)	Colour	Outside diameter (nm)	Length (μm)	Ash (wt.%)	Carbon content (%)	Part number
350	0.27	Black	< 8	30–10	< 1.5	> 98	GCM327

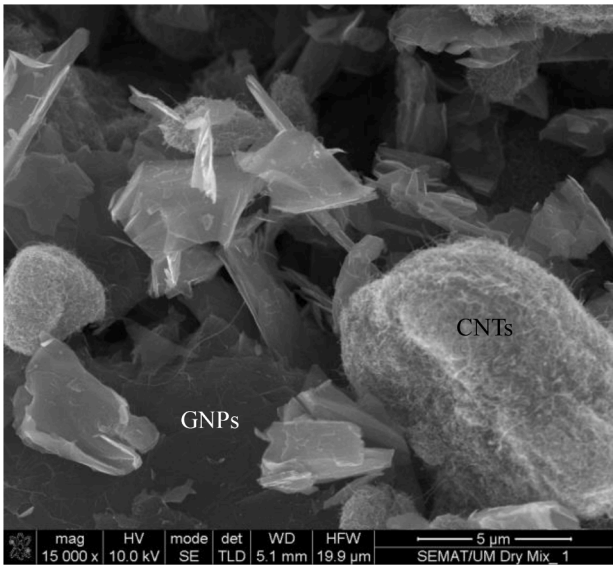

Fig. 1. Morphology of CNTs and GNPs in dry mixed state.

percolation threshold. The synergistic effects of CNT/GNP increase sensitivity and reduce the cost of production and the likelihood of porosity. However, to produce a sustainable self-sensing cementitious geocomposite (SCG) for field application, the low ductility behaviour must be addressed. Recent studies have indicated that incorporating fibres significantly improves the ductility and flexural behaviour of cementitious geocomposites [18–20]. Amongst various fibres used in cementitious composites, recycled glass and polypropylene fibres (GF and PP) have attracted substantial attention in different applications, mostly for their light weight, cost-effectiveness, and relative mechanical performance in terms of flexural and tensile moduli, and flexibility during processing and biodegradation [21–24]. Recently, a sustainable SCG was developed by the authors of this paper using hybrid CNT/GNP with the standard compaction method at optimum water content [25]. The effects of different concentrations of GF, PP, and ultra-high-molecular-weight polyethylene (UHMWPE) on microstructural and electrical performances of the composite were deeply investigated. Besides, the interfacial performance of the fibres-matrix such as bond strength, frictional bond strength, and chemical debonding energy was evaluated by various types of the test which indicates a different behaviour of these composites. Hence in the present study by knowing the reasons and origins of these differences, the geotechnical properties of the composite have been investigated and quantified.

Indeed in present study, in addition to the published research results by the authors in this subject [9,10,25–27], the effects of different concentrations of GF, PP, and ultra-high-molecular-weight polyethylene (UHMWPE) fibres on the mechanical, microstructural, durability, and piezoresistivity properties of SCGs are explored, more orientated toward geotechnical transport infrastructure applications. Due to the novelty of these composites, the relationships between the physical and hydro-mechanical properties of the reinforced composite were also studied to pave the design path of such composite in field application.

Table 2
Sand particle size distribution [9, 10].

Mesh size (mm)	0.08	0.16	0.5	1	1.6	2
Cumulative retained (%)	99±1	87±5	67±5	33±5	7 ± 5	0
Specific gravity (G_s)	2.67		Cu[a]	7.5	Cc[b]	1.8
Roundness (R)	0.45		Sphericity (S)	0.68	Regularity (ρ)	0.57

[a] Uniformity coefficient.
[b] Curvature coefficient.

The outcomes of this study are intended to contribute to the new era of smart infrastructures, including applications to rammed earth, ground improvement, and particularly in structural layers in transportation infrastructures, especially in critical zones such as transition zones. This self-sensing cementitious geocomposite can detect material damage, anticipate maintenance needs, and prevent structural failures.

2. Materials and methods

2.1. Raw materials

In this study, a multilayer GNP and multiwall CNT (MWCNT) were used as conductive fillers. The specifications of these carbon nanomaterials (CNMs) are presented in Table 1 [9,10]. The morphology of the hybrid GNPs/CNTs in the dry mixed state is depicted in Fig. 1.

A compatible noncovalent surfactant, Pluronic F-127, and tributyl phosphate (TBP, 97%) was used to disperse CNMs. In this study, CEN standard sand (ISO 679: 2009 and EN 196-1) and ordinary Portland cement type I (CEM I, 42.5R) were used for SCG fabrication. The physical properties of the sand are summarized in Table 2. Additional material specifications can be found in the literature [9,10,25–27].

A split film polypropylene (PP), alkali-resistant glass fibres (AR–GF), and an UHMWPE fibre called Dyneema with an average length of 12 mm were used for SCG reinforcement. The physical properties of the fibres are presented in Table 3. In this study, hydrofluoric acid (40%) and sulfuric acid (97%) were used for surface treatment of the fibres.

2.2. Specimen preparation

Although the hybrid combination of CNT/GNP can induce superior properties, the effective transfer of these characteristics to the geocomposite is strongly dependent on their dispersion status [28–32]. In this study, a compatible and effective method for hybrid CNT/GNP dispersion in aqueous suspension was used with 10% PF-127 (by weight of CNMs), with the addition of 50% TBP (by weight of surfactant) via 3 h of sonication (80 W output power and 45 kHz frequency) at 40 °C [9,10, 26,27]. To improve the surface condition, interaction, and adhesion with the cementitious matrix as well as their dispersion, the fibres were treated using a chemical method [33–37]. In this study, the GF were

Table 3
Physical properties of glass, UHMWPE, and polypropylene fibres.

Alkali-resistant glass fibre (AR–GF)						
Tensile strength (GPa)	Linear mass density of fibres (g/Km)	Density (kg/m^3)	Elastic modulus (GPa)	Elongation at break (%)	Length (mm)	Diameter (μm)
3.2	9600	2700	73.1	4.4	12	31
Ultra-high-molecular-weight polyethylene (UHMWPE) (Dyneema)						
Tensile strength (GPa)	Linear mass density of fibres (dtex)	Elastic modulus (GPa)	Elongation at break (%)	Length (mm)	Diameter (μm)	
3	440	10.3	5.6	12	14.5	
Polypropylene (split film)						
Tensile strength (MPa)	Density (kg/m^3)	Elastic modulus (GPa)	Elongation at break (%)	Length (mm)	Section dimensions (μm)	
54	910	4.31	15	12	36 * 640	

Table 4
Mix proportions of different self-sensing cementitious geocomposites.

Sample ID *	CNM (%)**	Glass fibre (%)	PP fibre (%)	UHMWPE fibre (%)	Cement (%)
SCG	0.17	–	–	–	10
SCGG (0.5%)	0.17	0.5	–	–	10
SCGG (1.0%)	0.17	1	–	–	10
SCGG (1.5%)	0.17	1.5	–	–	10
SCGP (0.5%)	0.17	–	0.5	–	10
SCGP (1.0%)	0.17	–	1	–	10
SCGP (1.5%)	0.17	–	1.5	–	10
SCGU (0.5%)	0.17	–	–	0.5	10
SCGU (1.0%)	0.17	–	–	1	10
SCGU (1.5%)	0.17	–	–	1.5	10

* All concentrations are represented by the weight of the dry sand.
** By equal proportion (1:1).

modified by immersion in 40% hydrofluoric acid for 18 h at 40 °C. The surfaces of the UHMWPE and PP fibres were treated with sulfuric acid and sodium dichromate solution for 24 h at 50 °C. The fibres were subsequently washed with water and dried at room temperature. This modification can lead to asperity on the fibre surface and likely cause a chemical reaction between the fibres and cement hydration products. Besides, the formation of functional groups on the surface of the fibres prevents them from agglomeration and improves their dispersion during the mixing process [25,38].

In soil stabilisation, the cement content usually varies by approximately 10% owing to the target strength of the sand–cement [39,40]. In this study, 10% cement (by weight of dry sand) was also utilized for SCG fabrication. The concentrations of the fibres were 0.5%, 1.0%, and 1.5% by weight of dry sand. First, the treated fibres and sand were added to a steel bowl and blended with a stainless-steel blade at a rotational speed of 140 rpm for 3.5 min. Then, cement was poured into the mixer and blended for 2 min at the same speed. Subsequently, CNM suspensions comprising 0.17% CNT/GNP (by weight of the sand and equal portions, 1:1), prepared with the ω_{opt} (for each fibre concentration), were sprayed into the mixture and blended at a speed of 285 rpm for 2.5 min.

All specimens in this study were prepared in 101.6 mm × 116.4 mm cylindrical moulds using the standard Proctor compaction method at optimum water content following ASTM D698. For specimens used in piezoresistivity tests, four square meshes of copper with dimensions of 50 mm × 50 mm were embedded as electrodes at distances of 38.8 mm and 19.4 mm from the middle of the specimen [9,10]. The specimens were identified by the variation in fibre type and dosage, as shown in Table 4.

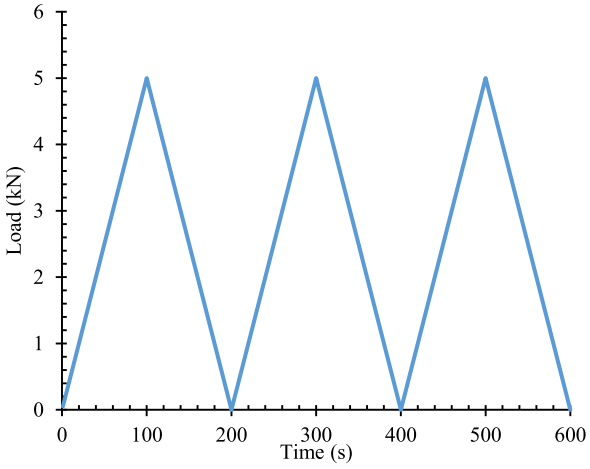

Fig. 2. Protocol for cyclic compression loading.

2.3. Mechanical, microstructural, and durability characterization

An unconfined compressive strength test was performed following the ASTM/D2166M standard to evaluate the mechanical characteristics of the cylindrical SCG specimens. The results were obtained using the mean of at least three specimens. Because the modulus of deformation for stabilised sand is typically expressed as the modulus at 50% of the peak stress ($E_{(50\%)}$) [41–44], the tangent moduli of reinforced SCGs with different fibre percentages were calculated to be 50% of the maximum compression stress. The effects of different fibre dosages on the maximum dry density and ω_{opt} were investigated according to the ASTM D698 standard. Thermal analysis was conducted to evaluate the effects of the fibres on the cement hydration process [27]. The fracture surfaces of the specimens were investigated using scanning electron microscopy (SEM) and energy-dispersive x-ray spectroscopy (EDX) [26,27]. An ultrasonic non-destructive test was performed for microstructural investigation following the BS EN 12,504–4 standard using two probes along the longitudinal axis. The weight loss percentage of the SCG specimens was measured as a criterion of cementitious geocomposite durability in freeze–thaw cycles. In this route, saturated specimens with similar dimensions were tested from 20 °C to 30 °C after 28 days of curing [9]. In addition, the relative dynamic modulus of elasticity was calculated for SCG specimens after climatic cycles [9,45]. The permeability of the SCG specimens was evaluated according to ASTM D2434–68.

2.4. Piezoresistivity measurement

A four-probe method was used to investigate the piezoresistivity of SCG specimens under cyclic compression loading with a direct current (DC) source [9,10]. The specimens with embedded electrodes were dried at 70 °C for 72 h after 28 days of hydration to ensure no moisture effects on electrical conductivity values. The variation in the gauge

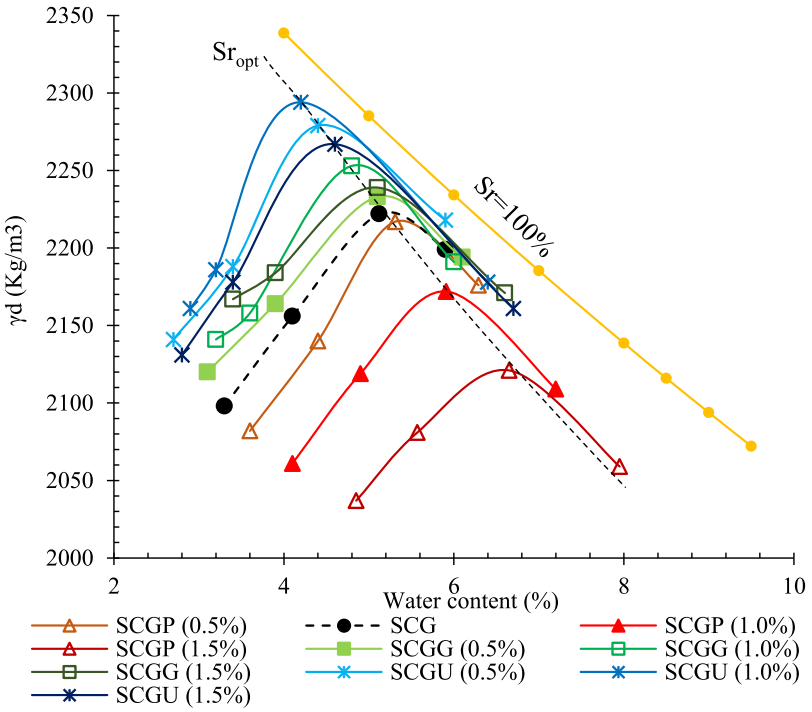

Fig. 3. Results of standard compaction Proctor tests for different SCGs.

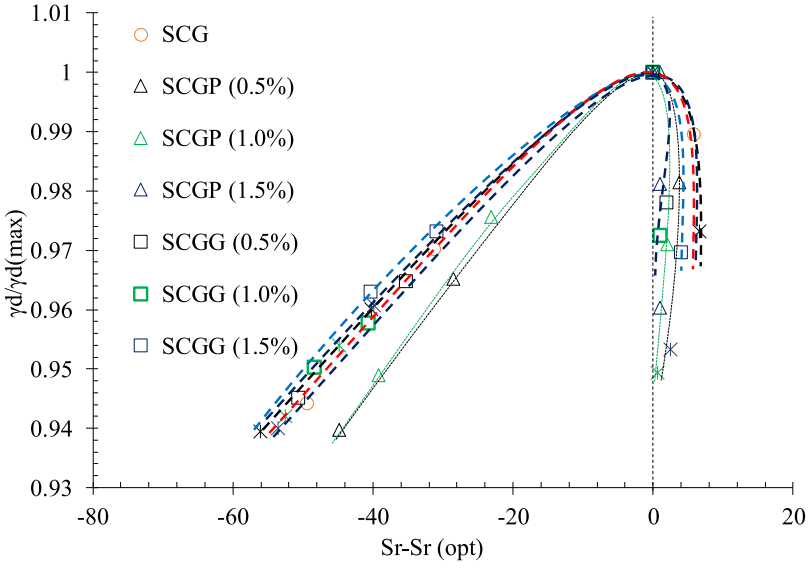

Fig. 4. Relationship between $\gamma_d/\gamma_{d(max)}$ and $Sr–Sr_{(opt)}$.

factors and fractional changes in electrical resistivity were calculated as the mean of at least four measurements. The protocol for cyclic compression loading is illustrated in Fig. 2.

3. Results

3.1. Compaction results and relevant microstructural investigations

3.1.1. Standard proctor compaction

The results of standard Proctor compaction tests on SCG and reinforced SCGs with different fibres are illustrated in Fig. 3. As shown in this Figure, despite all the different geocomposites, the maximum dry densities were obtained for approximately the same degree of saturation (Sr ≈ 85%), confirming the findings reported in a previous study [45]. Furthermore, the maximum dry density ($\gamma_{d(max)}$) was observed for the SCG with 1.0% UHMWPE fibres. This seems to be the optimal filling of particle voids, ensuring the best interlocking of particles. Excessive increase in the percentage produces a less dense material even more, significant than the specimen composed of 0.5% UHMWPE.

A similar trend was observed in the reinforced SCG specimens with GF; incorporating 1.0% GF as the optimum concentration of this fibre increased γ_d more than specimens SCGG (0.5%) and SCGG (1.5%). For PP-reinforced SCGs, incorporation of PP fibre into the specimens generally reduced γ_d. One of the main reasons for these trends may be the aspect ratio and section geometry of the fibres. The smaller dimensions of the UHMWPE fibres increased their performance in filling gaps between the sand grains. However, the rectangular shape of the PP cross-section produced an increase in the porosity and gaps between the

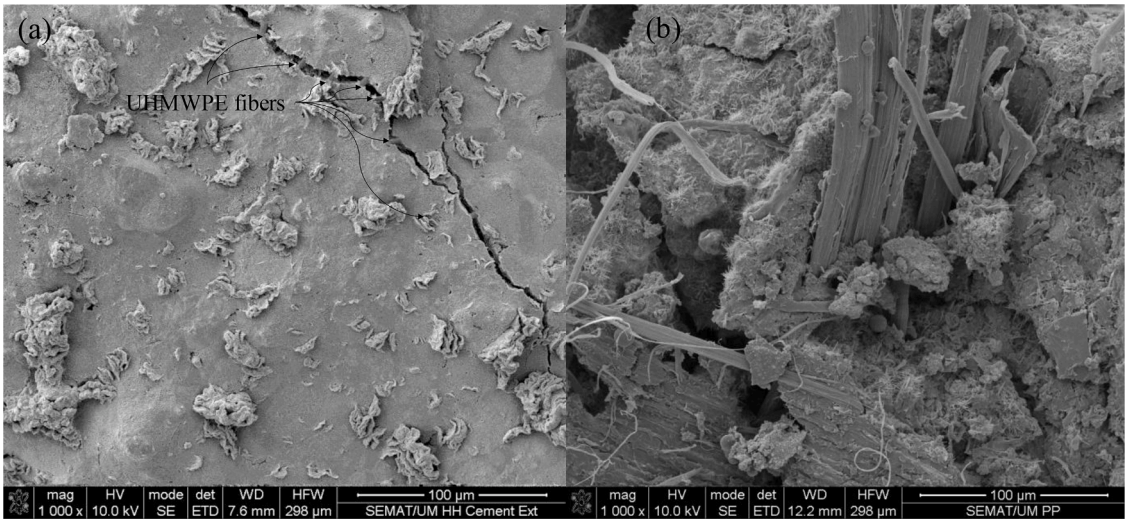

Fig. 5. a) Crack bridging (UHMWPE fibre); b) extruded fibre (PP fibre).

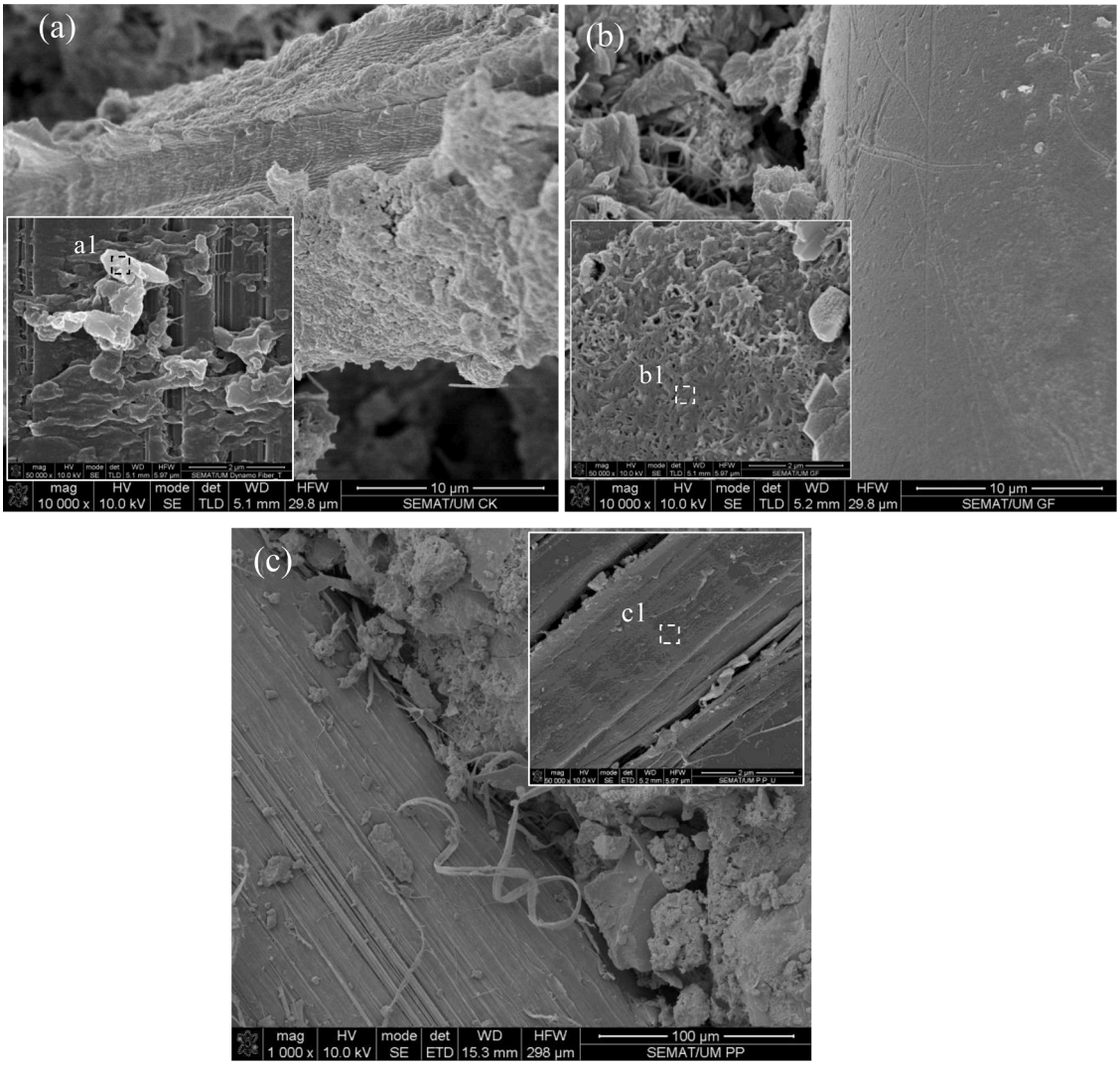

Fig. 6. Morphology of fibre surface: a) UHMWPE fibre; b) glass fibre; c) PP fibre (the marked areas in the SEM images indicate the areas selected for EDX analysis).

Table 5
Element analysis of extracted fibre surface.

Position	Elements (%)										
	C	O	Fe	Ca	Al	Si	S	Mg	Au	Mn	K
Fig. 6(a1)	7.94	35.47	0.91	28.12	1.14	23.36	0.51	0.94	0.79	1.1	0.68
Fig. 6(b1)	6.49	29.95	0.88	31.57	1.11	27.34	0.34	0.81	0.69	0.58	0.72
Fig. 6(c1)	43.74	12.96	1.24	15.38	1.92	17.58	2.19	2.27	0.83	0.49	1.16

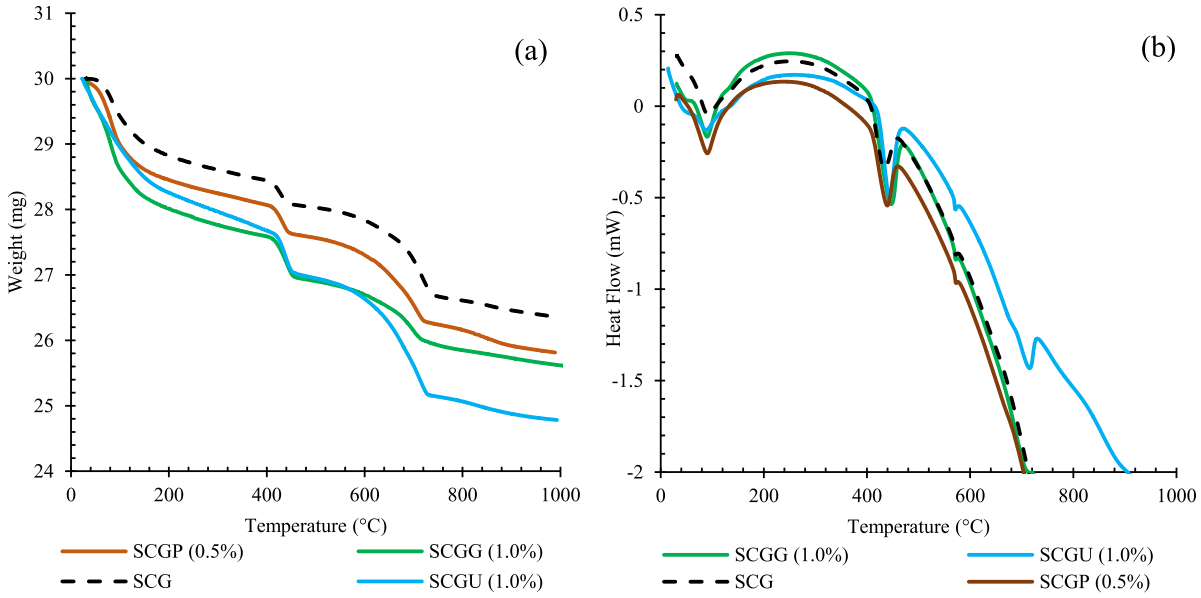

Fig. 7. Thermal analysis of different SCGs: a) Thermogravimetric analysis (TGA) spectra; b) Differential scanning calorimetry (DSC) curves.

sand grains, particularly at high dosages, which reduced γ_d and increased the optimum water content (ω_{Opt}). Increasing the gaps between the sand grains leads to a reduction in the degree of saturation, although the optimum degree of saturation $(Sr)_{opt}$ (defined as Sr obtained for $\gamma_{d(max)}$) is approximately the same as for the other soil types.

These interesting outcomes can also be represented by $\gamma_d/\gamma_{d(max)}$ vs. Sr–$(Sr)_{opt}$, which are more self-explanatory (Fig. 4). This unique relationship is consistent with recent studies [46,47], and is rather insensitive to variations in soil type. Consequently, it is more useful for practical earthworks applications, which is a major factor supporting the use of these novel materials in practice, mainly in the compacted layers of railroad foundations.

3.1.2. *Microstructural investigations*

The weakness in the physical properties of the composites can affect the mechanical and durability performance of the specimens. However, in the mechanical behaviour of fibre-reinforced composites, the bonding conditions of the fibre and matrix also play a crucial role. Indeed, in fibre-reinforced cementitious composites, the applied stresses are mobilised as frictional stresses on the surface of the fibres, preventing the formation and propagation of microcracks by a mechanism known as crack bridging (Fig. 5(a)). By increasing the load, frictional stresses also increase to reach the maximum friction bond strength of the fibres and cement matrix and/or tensile strength of the fibre.

In the case of weak interfacial properties, the fibres are incapable of restraining and harnessing the cracks. The fibres can be further extruded or pulled out from the cement matrix, increasing the crack opening and propagation (Fig. 5(b)). The interfacial properties of the fibres in cementitious composites are generally expressed by the frictional bond strength (τ_{fr}) and the chemical debonding energy (G_d), which depend on the physical and chemical conditions of the fibre surfaces, respectively.

From the literature [48–52], in addition to improving the frictional strength of the fibre/cement matrix by generating or deepening the surface roughness of the fibres, chemical treatment of the fibres can produce chemical functional groups, particularly oxygen groups, on the surface of the fibres. These functional groups participate in chemical reactions with cement hydration products and increase the chemical bonding energy of the fibre and cement matrix. The number and type of generated functional groups depend heavily on the chemical structure and composition of the fibre, the treatment agents, and methods. Generally, by evaluating the fibre morphologies and their interface with the cement matrix (Fig. 6), it is observed that the surfaces of the UHMWPE fibres and GF establish a more appropriate bond with hydration products and are surrounded by them. The surfaces of UHMWPE fibres have bumps and lesions with different textures that are properly bonded to them. The results of the chemical composition analysis of the fibre surfaces are summarised in Table 5. The results show that the chemical composition of the lesions is similar to that of CH and C-S-H [27,53], which contain high amounts of O, Ca, and Si. However, the PP fibre surfaces are free of such lesions and chemical compounds.

3.2. *Effects of fibres on cement hydration process*

To investigate the potential effects of fibres on the cement hydration process, thermogravimetric analysis (TGA) was conducted for SCGs reinforced by optimum concentrations of fibres; the results are presented in Fig. 7. The differential scanning calorimetry (DSC) results are presented in Fig. 7(b) for better observation of the temperature range associated with each weight decay. Generally, TGA is an analytical technique utilized to determine the fraction of volatile components by monitoring the weight change that occurs when a sample is heated at a constant rate.

In the TGA spectra, the first weight decay was from 0 °C to 105 °C, relative to the free water evaporation of the sample. The second weight

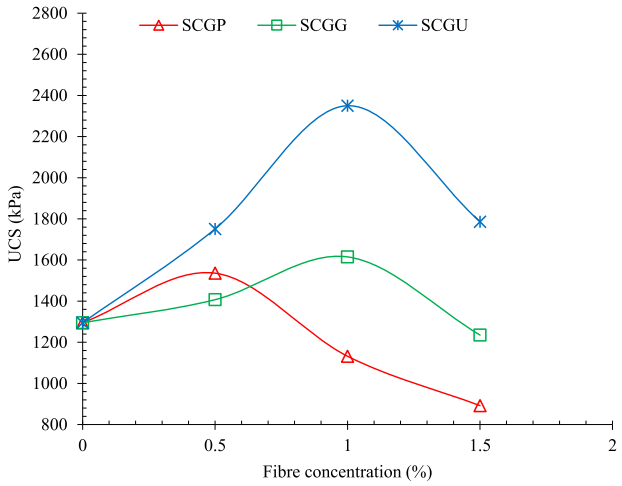

Fig. 8. Unconfined compressive strength (UCS) of different reinforced SCGs.

decay occurred from 105 °C to 400 °C, and was caused by dehydration of chemically bound water in cement hydration products such as C-S-H, Aft, C-A-S-H, and carbo-aluminates. The third weight decay was observed between 400 °C and 550 °C, and was related to the dihydroxylation of CH. The last weight decay occurred between 600 °C and 800 °C, and was attributed to carbonation of the clinker and calcium carbonate [54,55]. The TGA thermograms indicate that the incorporation of PP fibre generally did not have an effect on the amount of cement hydration product. However, using GF and UHMWPE fibres in the SCG produced a slight change in the amount of CH and C-S-H, which may be due to the functional groups formed on the surface of the fibres in chemical treatment. The presence of such functional groups, particularly oxygen groups, encourages and regulates the formation of cement hydration products on the fibre surfaces [27,53].

3.3. Mechanical and hydraulic performance

Unconfined compressive strength (UCS) tests were conducted to measure the mechanical properties of the different fibre-reinforced SCGs and compare them with the plain case. Although this test is not representative of stress paths in pavement structural layers, it is useful in soil improvement practice. The UCS results after 28 days of hydration are shown in Fig. 8. As expected from the physical properties, reinforcing SCG with fibres results in different UCS performances, depending on the type of fibres and their concentration in the composite.

As can be observed, the incorporating 0.5% PP fibres into the SCG produced an increase in the UCS of approximately 19%. However, excessive increases in the PP fibre dosage up to 1.0% and 1.5% reduced

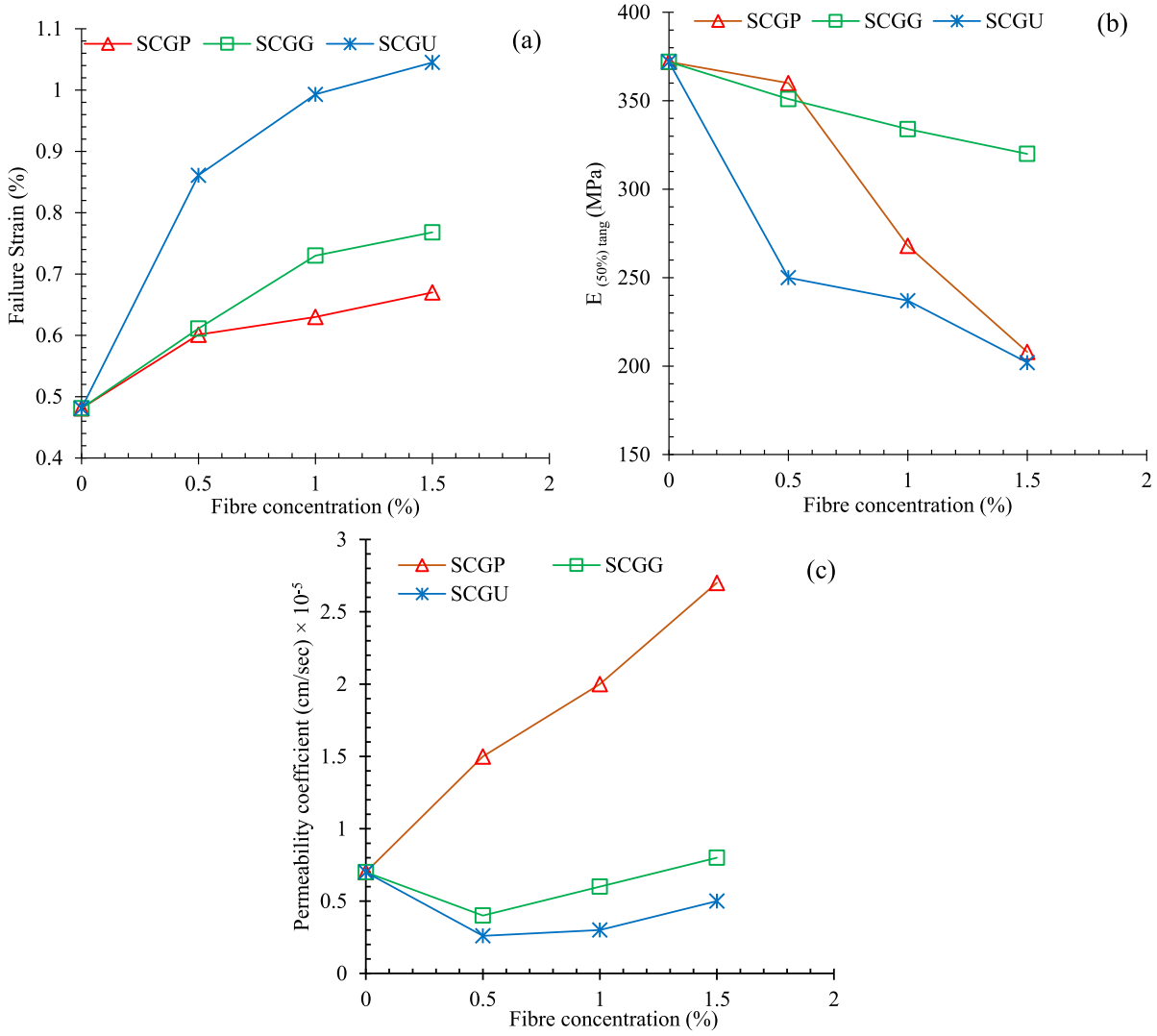

Fig. 9. The relationship between fibre concentration and: a) Failure strain; b) $E_{(50\%)}$; c) Permeability coefficient.

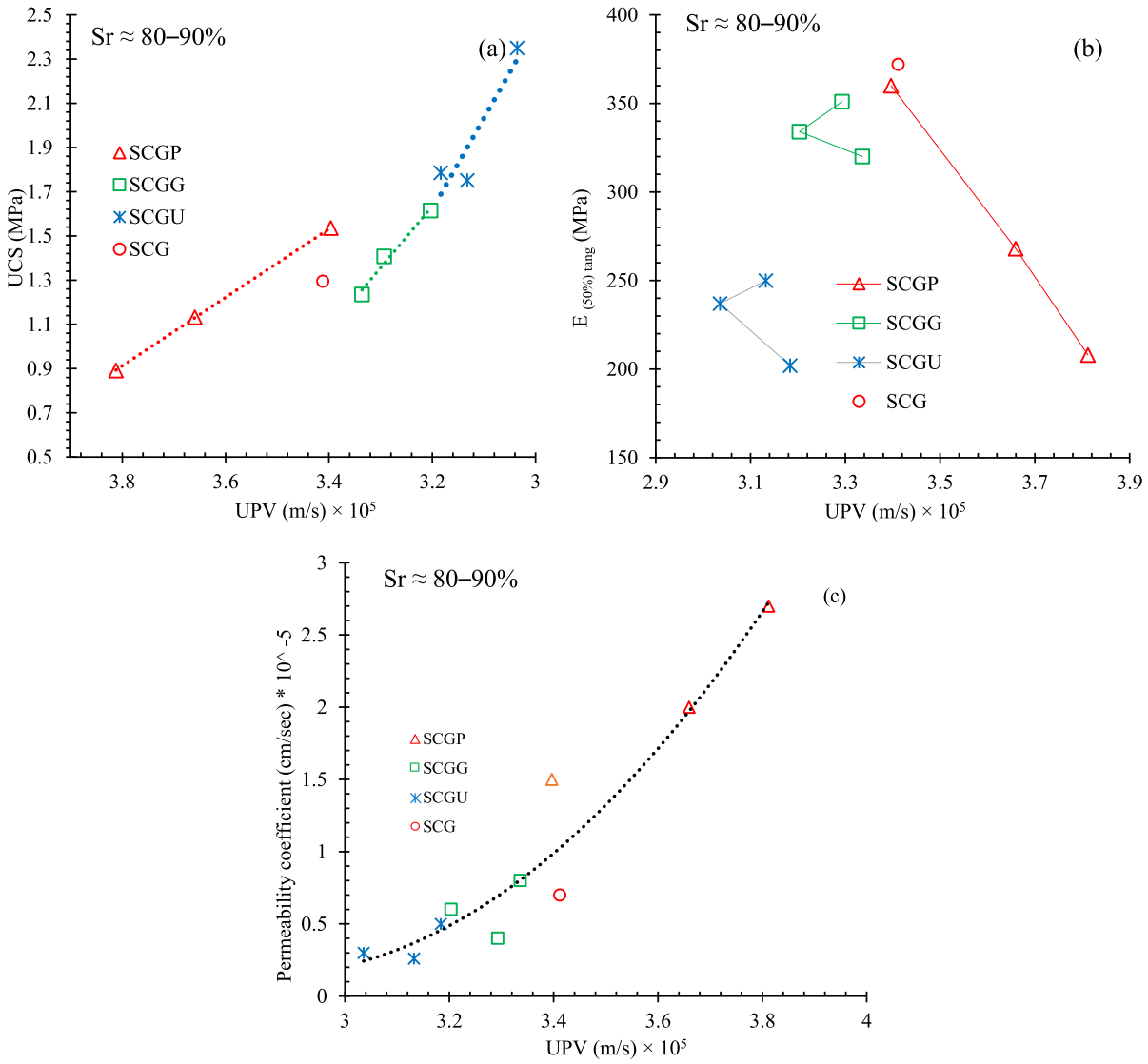

Fig. 10. Relationship between ultrasonic pulse velocity (UPV) and a) UCS; b) $E_{(50\%)tang}$; c) permeability coefficient.

the UCS by approximately 12% and 31%, respectively.

In the case of GF, the incorporating 0.5% and 1.0% GF into the SCG improved the UCS by approximately 9% and 25%, respectively. Increasing the dosage of GF by more than 1.0% led to a reduction in UCS by around 4%. Conversely, the incorporation of UHMWPE fibres into the SCG in all percentages in the range of 0.5% to 1.5% caused a UCS enhancement by around 35%, 82%, and 38% respectively.

Fig. 9 shows the influence of fibre type and concentration on the axial strain at failure (maximum stress), the tangent modulus at 50% of the peak stress ($E_{(50\%)}$), and the permeability coefficient of the specimens. Reinforcing SCG with 0.5%, 1.0%, and 1.5% PP fibres increased the failure strain by approximately 25%, 31%, and 40%, respectively. For GF, the increases were approximately 27%, 52%, and 60%; for UHMWPE fibres, the increases were 79%, 106%, and 117%, respectively.

For the moduli, reinforcing SCG with 0.5%, 1.0%, and 1.5% dosages of PP fibres reduced the $E_{(50\%)}$ by approximately 6%, 28%, and 44%, respectively. For these dosages of GF and UHMWPE fibres, the reductions were 8%, 12%, and 15%, and 33%, 36%, and 46%, respectively.

As shown in Fig. 9, the permeability coefficients of specimens containing 0.5%, 1.0%, and 1.5% PP fibres increased by approximately two, three, and four times, respectively, compared to the specimen composed of only CNMs. However, incorporation of the same UHMWPE fibre concentrations into SCG specimens reduced the permeability coefficient by approximately 62%, 57%, and 28%, respectively. For GF, specimens reinforced with 0.5% and 1.0% fibre showed a reduction in permeability coefficient of approximately 42% and 14%, respectively; while increasing the GF concentration to 1.5% increased the permeability coefficient by around 15%.

Fig. 10 presented some relationships between mechanical and hydraulic properties for the compaction tested conditions. To explain the different hydro-mechanical performances of the specimens, the relationships with the physical properties were studied, mainly related to compaction conditions (Fig. 11). The ultrasonic pulse velocity (UPV) results were also analysed because they correlate strongly with the UCS and dry density (Fig. 10 and Fig. 11). The relationship between the UPV, UCS, and $\gamma d_{(max)}$ is almost linear. However, as shown in Fig. 10(a), the slopes of the curves of specimens reinforced with UHMWPE are greater than those reinforced with GF and PP. For $E_{(50\%)\,tang}$, a similar behaviour was observed for the GF- and UHMWPE-reinforced composites. A reduction in the modulus was not consistently associated with a reduction in the UPV in the specimen. However, as shown in Fig. 10(c), increasing the permeability coefficient of the composite produced an

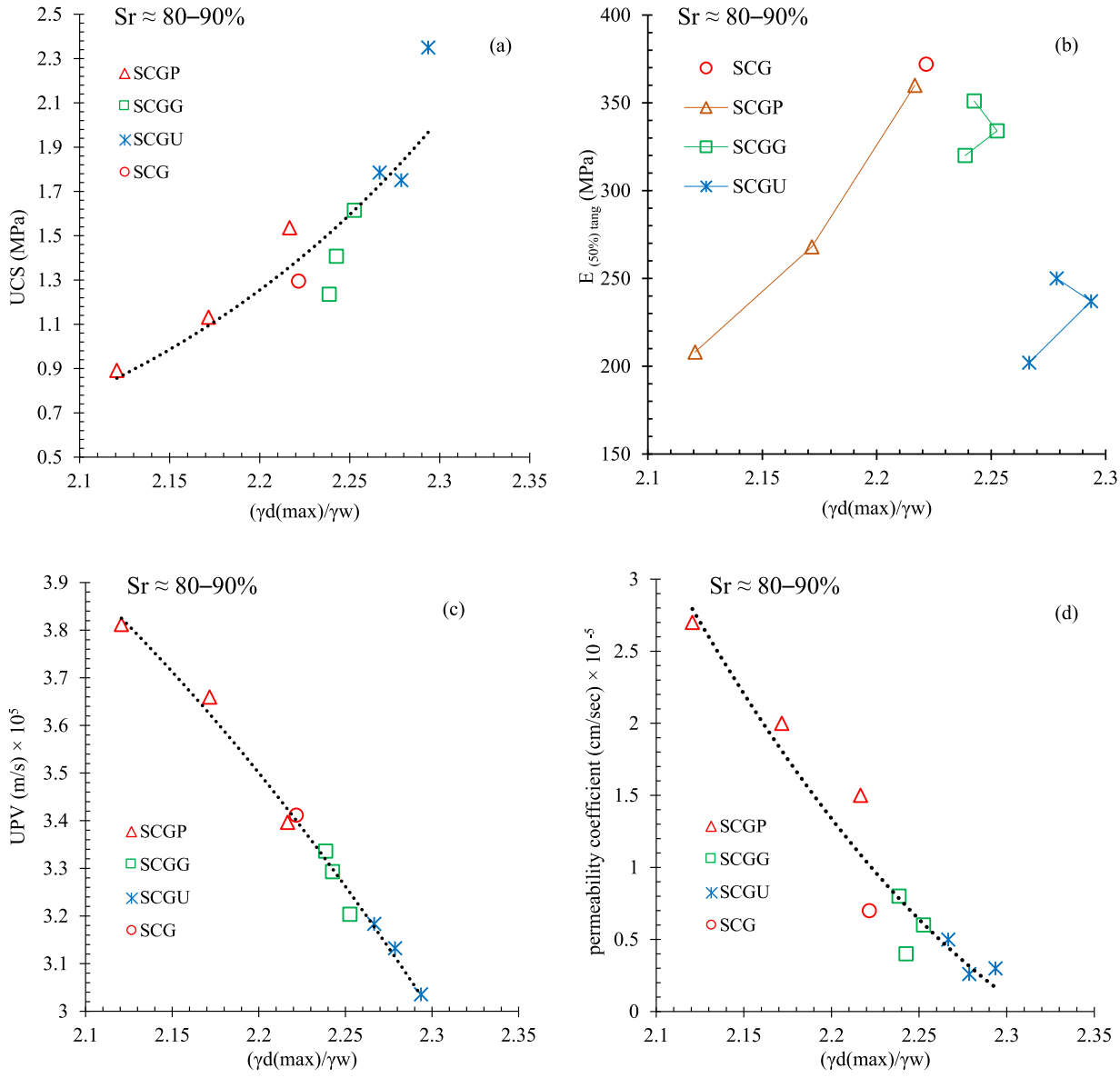

Fig. 11. Relationship between (γd(max)/γw) and a) UCS; b) E $_{(50\%)\ tang}$; c) UPV; d) permeability coefficient.

increase in the UPV.

As all tests were conducted at approximately the same optimal degree of saturation for each material, it is expected that the mechanical and hydraulic properties are strongly influenced by the dry density and type of fibre reinforcement, as shown in Fig. 11. For the quasi constant degree of saturation, there is a good correlation (unique trend) of strength (UCS), UPV and permeability coefficient with the maximum dry density, corroborating the finding in a previous study [9,45]. However, the geometric shape, mechanical properties, and interfacial properties of the fibre matrix seems to have a significant effect on the tangent deformability modulus [25], that may justify why a unique trend between (γ_d(max)/γ_w) and $E_{(50\%)\ tang}$ was not observed. It should be noted that based on the literature [56,57], irrespective of compaction energy level and composite type, in general the strength exhibits a sharp peak when the degree of saturation is slightly lower than the optimum degree of saturation. Consequently, the degree of saturation and its changes must be taken into account on the hydraulic behaviour, strength and stiffness, as well as on the piezoresistivity of cementitious geocomposites [10]. This aspect is out of the scope of this paper.

For design purposes in soil improvement, UCS and $E_{(50\%)tang}$ are required properties. The relationship between E $_{(50\%)\ tang}$ normalised by UCS and physical properties can be useful [58]. Fig. 12(a) and (b) show a well-defined correlation between the failure strain and elastic strain threshold (obtained from the stress–strain curves of UCS tests) and the ratio E $_{(50\%)\ tang}$ /UCS for 28 days. In line with the findings in [58] these relationships can be of very practical use in design. Indeed, a design engineer can easily predict the $E_{(50\%)\ tang}$ and elastic strain threshold for the design strain level based on conventional uniaxial compressive strength test results, particularly in the elastic region to reduce crack formation during the infrastructure service life. Fig. 13 shows the important role of the fibre matrix and its concentration in the geocomposite material in the serviceability limit state of the structure.

3.4. Durability of SCG

Generally, the durability of cementitious composites against environmentally aggressive agents, especially climatic cycles, is a most important consideration when developing a new composite [59,60]. To evaluate the durability and resistance of the specimen to climatic cycles, the weight loss percentage and relative dynamic modulus of elasticity

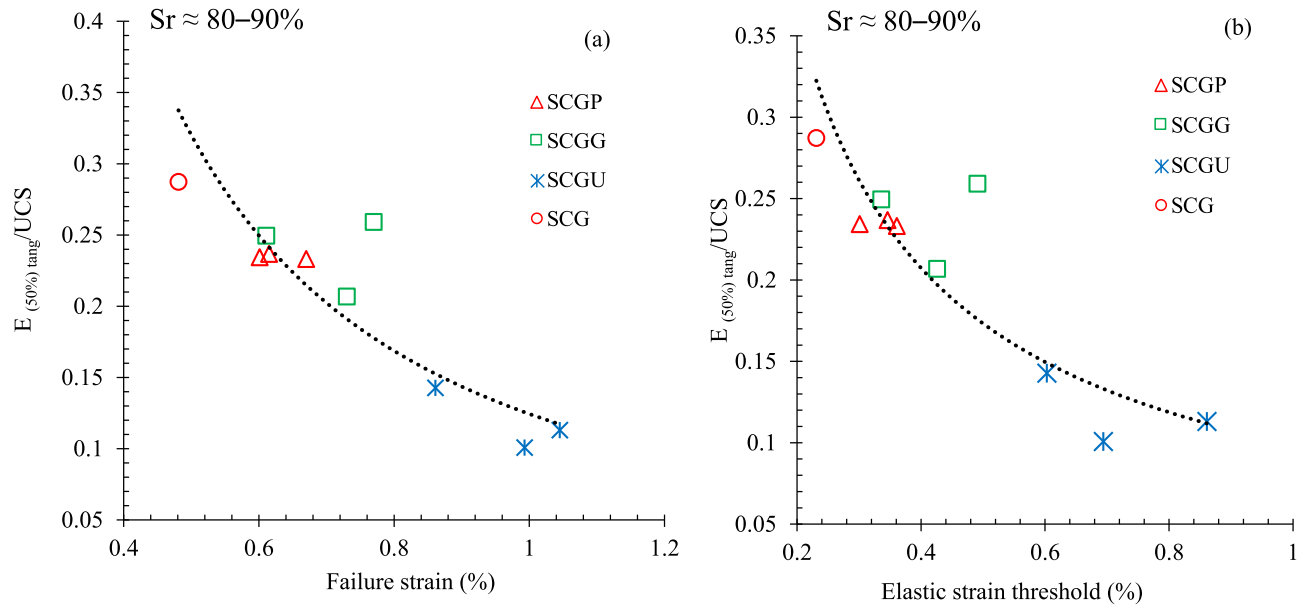

Fig. 12. Relationship between $E_{(50\%)\ tang}$ /UCS and a) failure strain; b) elastic strain threshold.

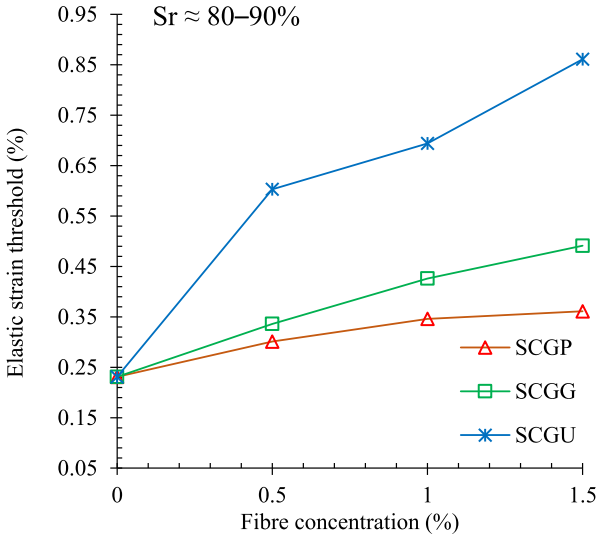

Fig. 13. Elastic strain threshold vs. fibre concentration.

for duplicate specimens were measured after 220 freeze–thaw cycles; the results are presented in Fig. 14. As expected, the smallest weight loss and greatest relative dynamic modulus were obtained for specimens reinforced with 1.0% UHMWPE, approximately 70% less than and 55% greater than that of plain SCG, respectively.

In the case of GF reinforcement, specimen SCGG (1.0%) showed a 31% reduction in weight loss and a 29% increase in relative dynamic modulus compared to plain SCG. However, incorporating PP fibres in increasing concentrations generally increased the weight loss of the specimen and reduced its relative dynamic modulus. The hydraulic conductivity of the composite, an important factor affecting the long-term performance of fibre-reinforced geomaterials, was investigated.

3.5. Electrical properties and piezoresistivity behaviour

3.5.1. Electrical conductivity

The electrical resistivity of the SCG specimens reinforced with different types and percentages of fibres was measured after 28 days and 90 days of hydration. It should be noted that all specimens were oven-dried at 70 °C for 72 h. The electrical resistivity results are shown in Fig. 15.

It is clear that incorporating non-conductive fibres into a conductive composite and increasing its concentration generally increases the electrical resistance. The fibres cut the random conductive paths formed by the CNMs and reduce the electrical conductivity of the composite. They can also potentially reduce quantum tunnelling effects and transfer electrons between the CNMs and existing ions, and in some cases, can change the percolation threshold. Incorporating 0.5%, 1.0%, and 1.5% PP fibres into SCGs increased the electrical resistivity by approximately 23%, 40%, and 115%, respectively. For GF reinforcement, the increases were approximately 14%, 49%, and 92%, respectively. For UHMWPE fibres, the electrical resistivity of the specimen with 0.5% fibre did not show a significant difference; the electrical resistivity of specimens containing 1.0% and 1.5% UHMWPE fibres increased by approximately 10% and 33%, respectively. The further increase in electrical resistance with PP fibres can be attributed to their larger dimensions and rectangular cross-section. As expected, the electrical conductivity of the specimens was reduced in the long term. Generally, by increasing the hydration period, the cement hydration products increase and spread in the pores, cutting off conductive paths. Cement hydration products in dry cases are often nonconductive and increase the electrical resistance. Increasing the density of hydration products produces a further reduction in the electrical conductivity of the composite over time.

As shown in Fig. 15, the electrical resistivity of the plain SCG after 90 days of curing was increased by approximately 173% compared with after 28 days. In SCG specimens reinforced with 0.5%, 1.0%, and 1.5% PP fibres, the electrical resistivity increased by approximately 196%, 191%, and 162% after 90 days, respectively, compared with after 28 days. For GF and UHMWPE fibres, the increases were approximately 186%, 167%, and 169%, and 248%, 177%, and 224%, respectively.

3.5.2. Piezoresistivity behaviour

The piezoresistivity behaviour of SCG specimens reinforced with different types and percentages of fibres under cyclic compression loading after 28 days is illustrated in Fig. 16. Negative values are observed for the fractional changes in electrical resistivity (FCR), which is consistent with previous studies [9,10,61–63]. Generally, the random conductive paths formed by CNMs become closer under compression loading. The electrical resistance of the specimen is reduced by reducing

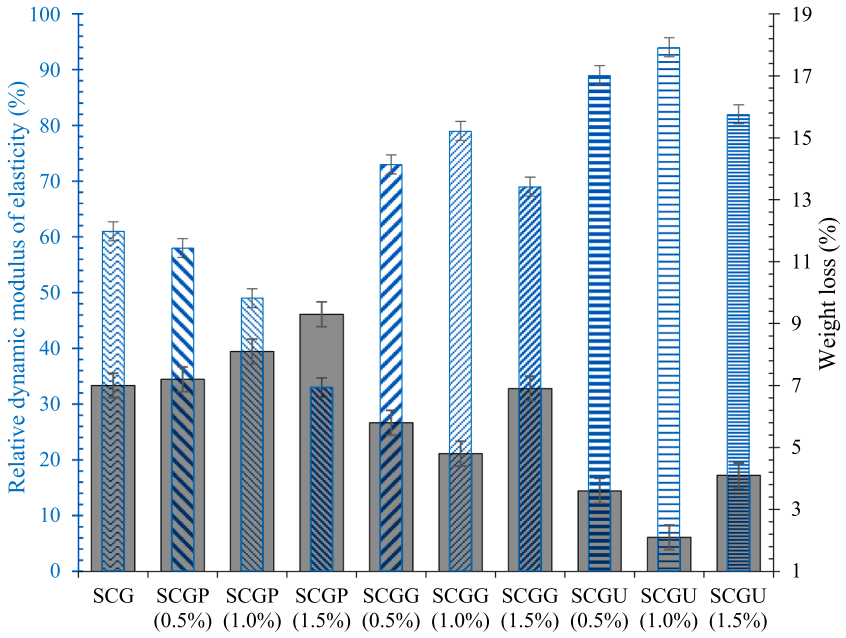

Fig. 14. Weight loss percentage and relative dynamic modulus of elasticity for duplicate specimens after 220 climatic cycles.

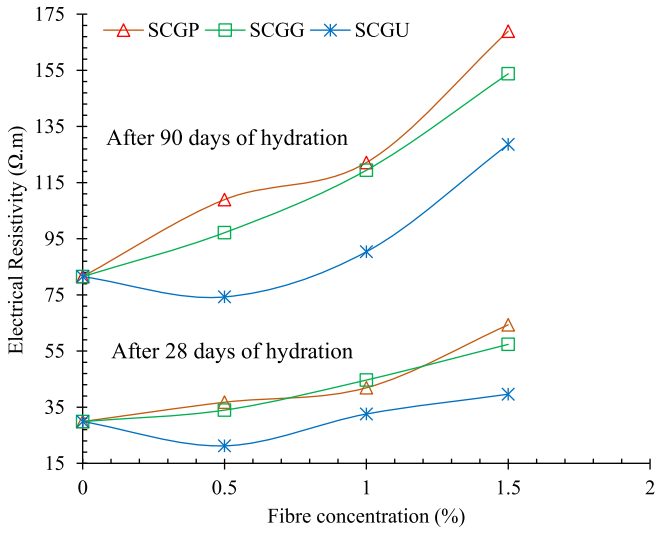

Fig. 15. Electrical resistivity of different reinforced specimens after 28 d and 90 d of hydration.

the distance between the conductive paths. The electron quantum tunnelling effects are also improved under compression loads, leading to increased electrical conductivity. Reducing the electrical resistivity relative to the initial values produces negative FCR values [64,65].

By increasing the load and strain in each cycle, the FCR was reduced; conversely, the FCR increased with decreasing load. Generally, reinforcing the specimen with fibre and increasing its concentration produced changes in the electrical resistivity and increased the FCR ranges due to the increasing deformation of the specimens. Increasing the deformation caused more strain under compression load and consequently produced changes in the shape and distance between random conductive paths that led to further changes in electrical resistance. However, an increase in deformation from excessive fibre produced large residual strain and residual FCR at the end of each cycle. The residual strain indicates the formation of nanoscale cracks in the microstructure of the composite. These cracks propagate over time with increasing loading cycles and cause microcracks, reducing the service life of the composite. As shown experimentally, incorporating an optimum dosage of fibre into the composite can increase its ductility.

To better interpret the relationship between FCR and axial strain, the correlation between FCR and strain for different reinforced SCGs is presented in Fig. 17. As can be observed, the power functions were found to better express the relation between these parameters. The slope of the UHMWPE fibre curve is steeper than that of the other specimens, indicating a higher sensitivity to axial strain. The curve of the GF-reinforced specimen had a lower slope, indicating a lower sensitivity.

3.5.3. *Gauge factors*

The gauge factor is calculated by dividing the FCR by the strain [9,10,66]. The gauge factor represents the sensitivity of the composite to strain. The gauge factors for different reinforced SCGs are shown in Fig. 18. The gauge factor of the plain SCG containing 0.17% CNMs was approximately 45. The maximum gauge factors were observed in the UHMWPE fibre-reinforced specimens; 0.5%, 1.0%, and 1.5% dosages in the plain SCG produced gauge factors of 52, 61, and 68, respectively. For PP- and GF-reinforced specimens, reinforcing SCG with 0.5%, 1.0%, and 1.5% fibres produced gauge factors of 44, 49, and 39, and 47, 42, and 41, respectively.

4. Conclusions

In this study, an emphasis in the geotechnical and piezoresistivity properties of a novel self-sensing cementitious geocomposite (SCG) with a hybrid CNT/GNP was put on throughout an extensive laboratory experimental program. The effects of different recycled fibres (PP, GF, and UHMWPE) on the microstructural, physical, mechanical, hydraulic, durability, and piezoresistivity performances of SCG were evaluated. Different concentrations of fibres were incorporated into the stabilised sand with 10% cement containing 0.17% CNT/GNP (by weight of the dry sand, 1:1). The specimens were fabricated using the standard Proctor compaction method at the optimum water content (degree of saturation 80–90%); the effects were investigated after 28 days of hydration using different test methods. The following conclusions can be drawn.

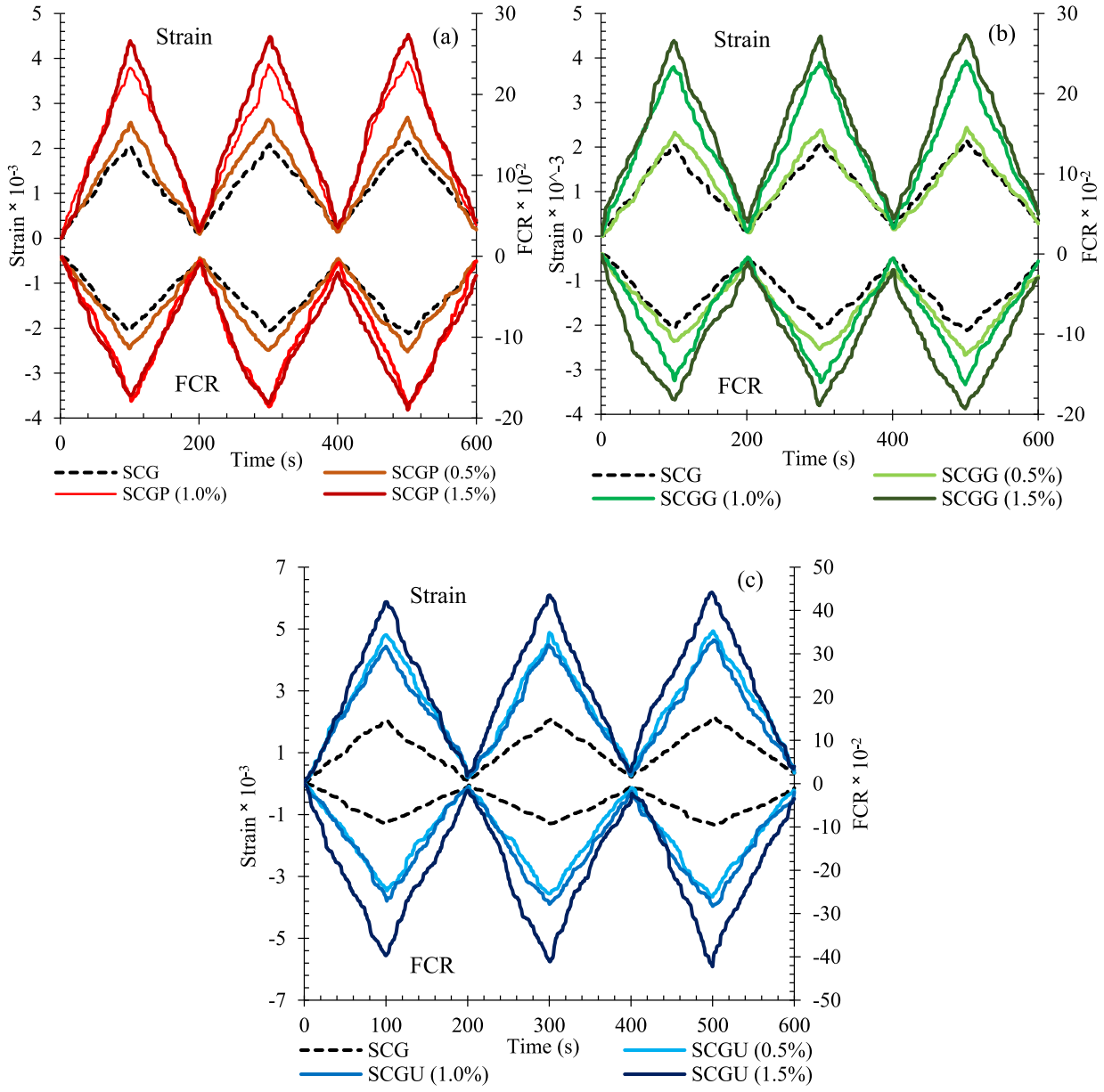

Fig. 16. FCR vs. strain for different SCG-reinforced specimens: a) reinforced with PP fibre; b) reinforced with GF; c) reinforced with UHMWPE fibre.

- The microstructural investigations indicated a better interaction between the cement matrix and UHMWPE fibres than with GF and PP fibres.
- Incorporating 1.0% GF and UHMWPE as optimum concentrations into the SCG compacted at optimum Standard Proctor conditions, increased the UCS by approximately 25% and 82%, respectively.
- Well-defined correlations between the mechanical, physical, and hydraulic properties of the fibre-reinforced composite were obtained experimentally that can be of practical interest to establish key geotechnical design parameters. Indeed, the quasi-unique relationship between the failure strain or the elastic strain threshold and the ratio $E_{(50\%)\ tang}$ /UCS for 28 days can be of very practical use in design.
- Reinforcing SCG with fibres increased its ductility; specimens with optimum concentrations of GF and UHMWPE showed $E_{(50\%)\ tang}$ values reduced by approximately 12% and 36%, respectively, as well as an increase of elastic strain threshold and failure strain, compared to the plain specimen.
- The geometric shape, mechanical characteristics and interfacial properties of the fibre matrix have a significant effect on the tangent deformability modulus, which may justify why a unique trend between ($\gamma d(max)/\gamma w$) and $E_{(50\%)\ tang}$ was not observed.
- Reinforcing SCG with optimum percentages of GF and UHMWPE fibres also increased the durability of the composite in climatic cycles and reduced the permeability. The smallest weight loss and a greater relative dynamic modulus were observed in the specimen reinforced with 1.0% UHMWPE, approximately 70% less than and 55% greater than that of plain SCG, respectively.
- The fibre-reinforced specimens showed proper piezoresistive behaviour under cyclic compression loading, indicating the high efficiency of this sustainable composite in infrastructure monitoring applications.
- Specimens with 0.5%, 1.0%, and 1.5% UHMWPE fibres had gauge factors of 52, 61, and 68, respectively; the gauge factor of the plain SCG containing 0.17% CNMs was approximately 45. For PP- and GF-reinforced composites, incorporating 0.5%, 1.0%, and 1.5% fibres

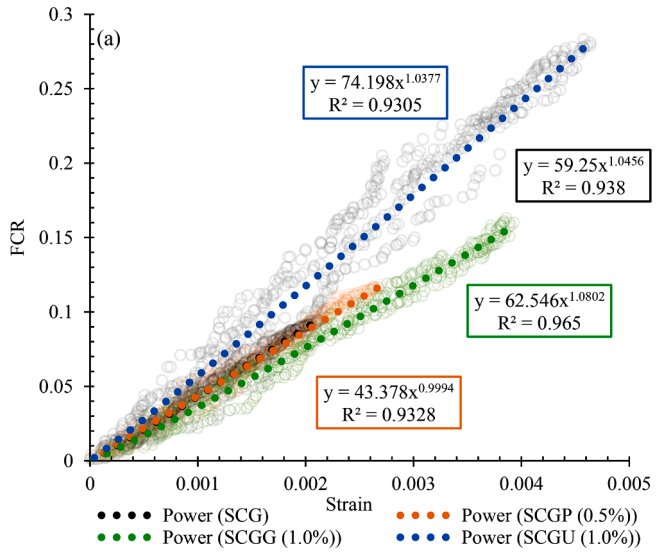

Fig. 17. Relationship between FCR and axial strain for SCG specimens reinforced with optimum percentages of PP, GF, and UHMWPE fibre.

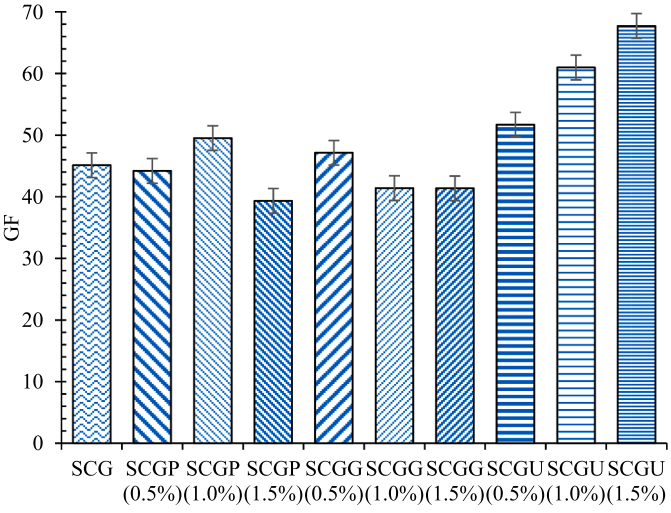

Fig. 18. Variation in gauge factor for different reinforced SCG specimens.

into the SCG produced gauge factors of 44, 49, and 39, and 47, 42, and 41, respectively.

In summary, we believe that these research findings contribute to the new era of smart geocomposite materials in sustainable intelligent transport infrastructures. Indeed, this is part of a laboratory work supporting a future railway track foundation demonstrator to be built on a Portuguese railway line in the framework of the project IN2TRACK3 under Shift2Rail Joint Undertaking.

CRediT authorship contribution statement

Mohammadmahdi Abedi: Conceptualization, Methodology, Validation, Formal analysis, Investigation, Resources, Data curation, Writing – original draft, Writing – review & editing, Visualization, Supervision, Project administration, Funding acquisition. **António Gomes Correia:** Conceptualization, Methodology, Validation, Formal analysis, Investigation, Resources, Data curation, Writing – original draft, Writing – review & editing, Visualization, Supervision, Project administration, Funding acquisition. **Raul Fangueiro:** Conceptualization, Methodology, Validation, Formal analysis, Investigation, Resources, Data curation, Writing – original draft, Writing – review & editing, Visualization, Supervision, Project administration, Funding acquisition.

CRediT authorship contribution statement

Mohammadmahdi Abedi: Conceptualization, Methodology, Validation, Formal analysis, Investigation, Resources, Data curation, Writing – original draft, Writing – review & editing, Visualization, Supervision, Project administration, Funding acquisition. **António Gomes Correia:** Conceptualization, Methodology, Validation, Formal analysis, Investigation, Resources, Data curation, Writing – original draft, Writing – review & editing, Visualization, Supervision, Project administration, Funding acquisition. **Raul Fangueiro:** Conceptualization, Methodology, Validation, Formal analysis, Investigation, Resources, Data curation, Writing – original draft, Writing – review & editing, Visualization, Supervision, Project administration, Funding acquisition.

Declaration of Competing Interest

The authors declare no conflicts of interest in this research.

Acknowledgement

This work was supported by the European Commission-Shiff2Rail Program under the project "IN2TRACK2–826255-H2020-S2RJU-2018/H2020-S2RJU CFM-2018". It was also partly financed by FCT/MCTES through National Funds (PIDDAC) under the R&D Unit Institute for Sustainability and Innovation in Engineering Structures (ISISE) under reference UIDB/04029/2020, and under the R&D Unit Centre for Textile Science and Technology (2C2T).

Data Availability Statement

Requests for all types of data used to support the findings of this study will be considered by the corresponding author after publication of this article, subject to permission from the owners.

References

[1] Y.-X. Zang, W. Gong, H. Xie, B.-L. Liu, H.-L. Chen, Chemical sand stabilization: a review of material, mechanism, and problems, Environ. Technol. Rev. 4 (1) (2015) 119–132.
[2] S. Paria, P.K. Yuet, Solidification–stabilization of organic and inorganic contaminants using portland cement: a literature review, Environ. Rev. 14 (4) (2006) 217–255.
[3] B. Yang, H. Li, H. Li, N. Ge, G. Ma, H. Zhang, et al., Experimental investigation on the mechanical and hydraulic properties of urease stabilized fine sand for fully permeable pavement, Int. J. Transp. Sci. Technol. (2020).
[4] F.I. Shalabi, J. Mazher, K. Khan, M. Alsuliman, I. Almustafa, W. Mahmoud, et al., Cement-stabilized waste sand as sustainable construction materials for foundations and highway roads, Materials (Basel) 12 (4) (2019) 600.
[5] P.K. Gautam, P. Kalla, A.S. Jethoo, R. Agrawal, H. Singh, Sustainable use of waste in flexible pavement: a review, Constr. Build. Mater. 180 (2018) 239–253.
[6] M. Joel, I.O. Agbede, Mechanical-cement stabilization of laterite for use as flexible pavement material, J. Mater. Civil Eng. 23 (2) (2011) 146–152.
[7] M. Arjomand, M. Abedi, M. Gharib, M. Damghani, An Experimental study on Geogrid with geotextile effects aimed to improve clayey soil, Int. J. Eng. 32 (5) (2019) 685–692.
[8] S. Rana, P. Subramani, R. Fangueiro, A.G. Correia, A review on smart self-sensing composite materials for civil engineering applications, AIMS Mater. Sci. 3 (2) (2016) 357–379.
[9] M. Abedi, R. Fangueiro, A. Gomes Correia, Ultra-sensitive affordable cementitious composite with high mechanical and microstructural performances by hybrid CNT/GNP, Materials (Basel) 13 (16) (2020) 3484.
[10] M. Abedi, R. Fangueiro, A.G. Correia, Development of a novel multifunctional cementitious-based geocomposite by the contribution of CNT and GNP, Nanomaterials 11 (4) (2021) 961.
[11] B. Han, S. Ding, X. Yu, Intrinsic self-sensing concrete and structures: a review, Measurement 59 (2015) 110–128.
[12] W. Dong, W. Li, Z. Tao, K. Wang, Piezoresistive properties of cement-based sensors: review and perspective, Constr. Build. Mater. 203 (2019) 146–163.
[13] R. Guo, Y. Suo, H. Xia, Y. Yang, Q. Ma, F. Yan, Study of piezoresistive behavior of smart cement filled with graphene oxide, Nanomaterials 11 (1) (2021) 206.

[14] L. Duan, A.Z. Abdullah. Effects of Moisture on Mechanical and Piezoresistive Properties of Cement Composites Containing Carbon Fiber During Long Age. EDP Sciences. 03061.
[15] L. Wang, F. Aslani, Mechanical properties, electrical resistivity and piezoresistivity of carbon fibre-based self-sensing cementitious composites, Ceram. Int. 47 (6) (2021) 7864–7879.
[16] W. Dong, W. Li, K. Wang, S.P. Shah, Physicochemical and Piezoresistive properties of smart cementitious composites with graphene nanoplates and graphite plates, Constr. Build. Mater. 286 (2021), 122943.
[17] W. Dong, W. Li, X. Zhu, D. Sheng, S.P. Shah, Multifunctional cementitious composites with integrated self-sensing and hydrophobic capacities toward smart structural health monitoring, Cement Concr. Compos. 118 (2021), 103962.
[18] A. Khajeh, R.J. Chenari, M. Payan, A simple review of cemented non-conventional materials: soil composites, Geotech. Geol. Eng. 38 (2) (2020) 1019–1040.
[19] D.Y. Yoo, S. Kim, G.-J. Park, J.-J. Park, S.-W. Kim, Effects of fiber shape, aspect ratio, and volume fraction on flexural behavior of ultra-high-performance fiber-reinforced cement composites, Compos. Struct. 174 (2017) 375–388.
[20] F. Wu, L. Xu, Y. Chi, Y. Zeng, F. Deng, Q. Chen, Compressive and flexural properties of ultra-high performance fiber-reinforced cementitious composite: the effect of coarse aggregate, Compos. Struct. 236 (2020), 111810.
[21] S.-S. Park, Unconfined compressive strength and ductility of fiber-reinforced cemented sand, Constr. Build. Mater. 25 (2) (2011) 1134–1138.
[22] N.C. Consoli, F. Zortéa, M. de Souza, L. Festugato, Studies on the dosage of fiber-reinforced cemented soils, J. Mater. Civil Eng. 23 (12) (2011) 1624–1632.
[23] J. Liu, Z. Chen, Z. Song, Y. Bai, W. Qian, J. Wei, et al., Tensile behavior of polyurethane organic polymer and polypropylene fiber-reinforced sand, Polymers (Basel) 10 (5) (2018) 499.
[24] J.J. Murray, J.D. Frost, Y. Wang, Behavior of a sandy silt reinforced with discontinuous recycled fiber inclusions, Transp. Res. Rec. 1714 (1) (2000) 9–17.
[25] M. Abedi, R. Fangueiro, A. Gomes Correia, Innovative self-sensing fiber-reinforced cemented sand with hybrid CNT/GNP, Smart Mater. Struct. 30 (10) (2021), 105034.
[26] M. Abedi, R. Fangueiro, A.G. Correia, An Effective Method for Hybrid CNT/GNP Dispersion and Its effects on the mechanical, microstructural, thermal, and electrical properties of multifunctional cementitious composites, J. Nanomater. 2020 (2020).
[27] M. Abedi, R. Fangueiro, A. Camões, A.G. Correia, Evaluation of CNT/GNP's synergic effects on the mechanical, microstructural, and durability properties of a cementitious composite by the novel dispersion method, Constr. Build. Mater. 260 (2020), 120486.
[28] S. Parveen, S. Rana, R. Fangueiro, A review on nanomaterial dispersion, microstructure, and mechanical properties of carbon nanotube and nanofiber reinforced cementitious composites, J. Nanomater. 2013 (2013).
[29] J.-L. Phua, P.-L. Teh, S.A. Ghani, C.-K. Yeoh, Effect of heat assisted bath sonication on the mechanical and thermal deformation behaviours of graphene nanoplatelets filled epoxy polymer composites, Int. J. Polym. Sci. 2016 (2016).
[30] A. Ibrahim, S. Ridha, A. Amer, R. Shahari, T. Ganat, Influence of degree of dispersion of noncovalent functionalized graphene nanoplatelets on rheological behaviour of aqueous drilling fluids, Int. J. Chem. Eng. 2019 (2019).
[31] S.-T. Kang, J.-Y. Seo, S.-H. Park, The characteristics of CNT/cement composites with acid-treated MWCNTs, Adv. Mater. Sci. Eng. 2015 (2015).
[32] M. Ghazi, M. Pourhajibagher, A. Bahador, N. Chiniforush, S. Dadpour, Y. Dadpour, Evaluation of adding Nanosized natural Zeolite to photodynamic therapy against P. gingivalis biofilm on titanium disks, Photodiagn. Photodyn. Ther. (2021), 102519.
[33] X. Fu, W. Lu, D.D.L. Chung, Improving the bond strength between carbon fiber and cement by fiber surface treatment and polymer addition to cement mix, Cement Concr. Res. 26 (7) (1996) 1007–1012.
[34] B.A. Proctor, B. Yale, Glass fibres for cement reinforcement, Philos. Trans. R. Soc. Lond. Ser. A Math. Phys. Sci. 294 (1411) (1980) 427–436.
[35] R. Pratama, G. Ramahdita, A.Z. Syahrial, M. Chalid, Feasibility study of chemical treatments on sorghum fibres for compatibility enhancement in polypropylene composites, Trans. Tech. Publ. (2018) 70–77.
[36] B. Mobasher, V. Dey, J. Bauchmoyer, H. Mehere, S. Schaef, Reinforcing efficiency of micro and macro continuous polypropylene fibers in cementitious composites, Appl. Sci. 9 (11) (2019) 2189.
[37] A. Peled, H. Guttman, A. Bentur, Treatments of polypropylene fibres to optimize their reinforcing efficiency in cement composites, Cement Concr. Compos. 14 (4) (1992) 277–285.
[38] M. Abedi, R. Fangueiro, A.G. Correia, Effects of multiscale carbon-based conductive fillers on the performances of a self-sensing cementitious geocomposite, J. Build. Eng. 43 (2021), 103171.
[39] X. Wei, T. Ku, New design chart for geotechnical ground improvement: characterizing cement-stabilized sand, Acta Geotech. 15 (4) (2020) 999–1011.
[40] G. Vinoth, S.W. Moon, J. Moon, T. Ku, Early strength development in cement-treated sand using low-carbon rapid-hardening cements, Soils Found. 58 (5) (2018) 1200–1211.
[41] Y. Yilmaz, V. Ozaydin, Compaction and shear strength characteristics of colemanite ore waste modified active belite cement stabilized high plasticity soils, Eng. Geol. 155 (2013) 45–53.
[42] Y. Yilmaz, Experimental investigation of the strength properties of sand–clay mixtures reinforced with randomly distributed discrete polypropylene fibers, Geosynth. Int. 16 (5) (2009) 354–363.
[43] A.A.S. Correia, M.G. Rasteiro, Nanotechnology applied to chemical soil stabilization, Procedia Eng 143 (2016) 1252–1259.
[44] A.G. Correia, T. Valente, J. Tinoco, J. Falcão, J. Barata, D. Cebola, et al., Evaluation of mechanical properties of jet-grouting columns using different test methods, in: Proceedings of the 17th International Conference on Soil Mechanics and Geotechnical Engineering: The Academia and Practice of Geotechnical Engineering, 2009, pp. 2169–2171.
[45] X. Wang, I. Rhee, Y. Wang, Y. Xi, Compressive strength, chloride permeability, and freeze-thaw resistance of MWNT concretes under different chemical treatments, Sci. World J. 2014 (2014).
[46] F. Tatsuoka, A.G. Correia, Importance of controlling the degree of saturation in soil compaction, Procedia Eng. 143 (2016) 556–565.
[47] F. Tatsuoka, A.G. Correia. On Frequent Evaluation of Compacted States and Soil Properties By Soil Stiffness Index Measurements. Springer. 596–614.
[48] A.M. López-Buendía, M.D. Romero-Sánchez, V. Climent, C. Guillem, Surface treated polypropylene (PP) fibres for reinforced concrete, Cement Concr. Res. 54 (2013) 29–35.
[49] L.J. Larner, K. Speakman, A.J. Majumdar, Chemical interactions between glass fibres and cement, J. Non Cryst Solids 20 (1) (1976) 43–74.
[50] L. Akand, M. Yang, X. Wang, Effectiveness of chemical treatment on polypropylene fibers as reinforcement in pervious concrete, Constr. Build. Mater. 163 (2018) 32–39.
[51] M. Le Troëdec, C.S. Peyratout, A. Smith, T. Chotard, Influence of various chemical treatments on the interactions between hemp fibres and a lime matrix, J. Eur. Ceram. Soc 29 (10) (2009) 1861–1868.
[52] N.L. Lovata, M.F. Fahmy, Interfacial bond study of a chemically treated polypropylene fibre-reinforced concrete, Constr. Build. Mater. 1 (2) (1987) 83–87.
[53] S. Lv, Y. Ma, C. Qiu, T. Sun, J. Liu, Q. Zhou, Effect of graphene oxide nanosheets of microstructure and mechanical properties of cement composites, Constr. Build. Mater. 49 (2013) 121–127.
[54] L.P. Singh, D. Ali, U. Sharma, Studies on optimization of silica nanoparticles dosage in cementitious system, Cement Concr. Composit. 70 (2016) 60–68.
[55] L.P. Singh, D. Ali, I. Tyagi, U. Sharma, R. Singh, P. Hou, Durability studies of nano-engineered fly ash concrete, Constr. Build. Mater. 194 (2019) 205–215.
[56] F. Tatsuoka, S. Furusawa, T. Kataoka, K. Watanabe, T. Lohani, Strength and stiffness of compacted cement-mixed gravelly soil controlled by the degree of saturation, in: Proceedings of 19th ICSMGE, Seoul, 2017, pp. 1253–1256.
[57] L. Kongsukprasert, F. Tatsuoka, M. Tateyama, Several factors affecting the strength and deformation characteristics of cement-mixed gravel, Soils Found. 45 (3) (2005) 107–124.
[58] A.G. Correia, J. Tinoco, Advanced tools and techniques to add value to soil stabilization practice, Innov. Infrastruct. Solut. 2 (1) (2017) 1–9.
[59] H. Eskandari-Naddaf, A. Ziaei-Nia, Simultaneous effect of nano and micro silica on corrosion behaviour of reinforcement in concrete containing cement strength grade of C-525, Procedia Manuf. 22 (2018) 399–405.
[60] J de J.A. Baldovino, R.L. dos Santos Izzo, J.L. Rose, Effects of freeze–thaw cycles and porosity/cement index on durability, strength and capillary rise of a stabilized silty soil under optimal compaction conditions, Geotech. Geol. Eng. 39 (1) (2021) 481–498.
[61] B. Han, X. Yu, J. Ou, Effect of water content on the piezoresistivity of MWNT/cement composites, J. Mater. Sci. 45 (14) (2010) 3714–3719.
[62] A. Dinesh, S.T. Sudharsan, S. Haribala, Self-sensing cement-based sensor with carbon nanotube: fabrication and properties–A review, Mater. Today: Proc. (2021).
[63] C. Vipulanandan, A. Mohammed, Smart cement compressive piezoresistive, stress-strain, and strength behavior with nanosilica modification, J. Test Eval. 47 (2) (2018) 1479–1501.
[64] D.-Y. Yoo, I. You, H. Youn, S.-J. Lee, Electrical and piezoresistive properties of cement composites with carbon nanomaterials, Constr. Build. Mater. 52 (24) (2018) 3325–3340.
[65] L. Wang, F. Aslani, Piezoresistivity performance of cementitious composites containing activated carbon powder, nano zinc oxide and carbon fibre, Constr. Build. Mater. 278 (2021), 122375.
[66] M. Abedi, R. Fangueiro, A. Gomes Correia, A review of intrinsic self-sensing cementitious composites and prospects for their application in transport infrastructures, Constr. Build. Mater. 310 (2021), 125139.